Journal of Applied Physics

Thermal conductivity of $(Ge_2Sb_2Te_5)_{1-x}C_x$ phase change films

Cite as: J. Appl. Phys. **128**, 155106 (2020); https://doi.org/10.1063/5.0023476
Submitted: 29 July 2020 . Accepted: 26 September 2020 . Published Online: 19 October 2020

Ethan A. Scott, Elbara Ziade, Christopher B. Saltonstall, Anthony E. McDonald, Mark A. Rodriguez, Patrick E. Hopkins, Thomas E. Beechem, and David P. Adams

Journal of Applied Physics ARTICLE scitation.org/journal/jap

Thermal conductivity of $(Ge_2Sb_2Te_5)_{1-x}C_x$ phase change films

Cite as: J. Appl. Phys. **128**, 155106 (2020); doi: 10.1063/5.0023476
Submitted: 29 July 2020 · Accepted: 26 September 2020 ·
Published Online: 19 October 2020

Ethan A. Scott,[1,2] Elbara Ziade,[1] Christopher B. Saltonstall,[1] Anthony E. McDonald,[1] Mark A. Rodriguez,[1] Patrick E. Hopkins,[2,3,4] Thomas E. Beechem,[1,5] and David P. Adams[1,a)]

AFFILIATIONS

[1]Sandia National Laboratories, Albuquerque, New Mexico 87185, USA
[2]Department of Mechanical and Aerospace Engineering, University of Virginia, Charlottesville, Virginia 22904, USA
[3]Department of Materials Science and Engineering, University of Virginia, Charlottesville, Virginia 22904, USA
[4]Department of Physics, University of Virginia, Charlottesville, Virginia 22904, USA
[5]Center for Integrated Nanotechnologies, Albuquerque, New Mexico 87185, USA

Note: This paper is part of the Special Topic on Phase-Change Materials: Syntheses, Fundamentals, and Applications.
a)Author to whom correspondence should be addressed: dpadams@sandia.gov

ABSTRACT

Germanium–antimony–telluride has emerged as a nonvolatile phase change memory material due to the large resistivity contrast between amorphous and crystalline states, rapid crystallization, and cyclic endurance. Improving thermal phase stability, however, has necessitated further alloying with optional addition of a quaternary species (e.g., C). Here, the thermal transport implications of this additional species are investigated using frequency-domain thermoreflectance in combination with structural characterization derived from x-ray diffraction and Raman spectroscopy. Specifically, the room temperature thermal conductivity and heat capacity of $(Ge_2Sb_2Te_5)_{1-x}C_x$ are reported as a function of carbon concentration ($x \leq 0.12$) and anneal temperature ($T \leq 350\,^{\circ}C$) with results assessed in reference to the measured phase, structure, and electronic resistivity. Phase stability imparted by the carbon comes with comparatively low thermal penalty as materials exhibiting similar levels of crystallinity have comparable thermal conductivity despite the addition of carbon. The additional thermal stability provided by the carbon does, however, necessitate higher anneal temperatures to achieve similar levels of structural order.

I. INTRODUCTION

GeSbTe-based solid solutions are chalcogenide materials that reversibly change phase in response to sufficient alterations in temperature that are commonly realized with a pulsed laser or current.[1,2] A phase change modifies the atomic arrangement and thus the material's electronic and optical properties. The reversible property changes, in turn, lend themselves toward several applications.[1,3] Particular stoichiometries, namely, $Ge_2Sb_2Te_5$ and $Ge_8Sb_2Te_{11}$, for example, have long been used in phase change memory applications such as re-writable disks, which benefit from high speeds of crystallization, long cycling lifetime, and favorable stability.[3]

The same properties that make $Ge_2Sb_2Te_5$ attractive as a phase change material suggest its applicability for non-volatile computer memory as well.[4] However, for practical use in phase-change random access memory (PRAM), a number of improvements are necessary, including the need for reduced set/reset (crystallization/amorphization) currents and increased thermal stability of the amorphous phase.[5] Increased phase stability, in turn, is associated with an increase in the temperature of crystallization that, if realized, could facilitate data retention at higher temperatures and thus the development of $Ge_2Sb_2Te_5$ PRAM for extreme environments.[5]

To this end, several quaternary $Ge_2Sb_2Te_5$ solutions have been pursued via the addition of Se, N, O, Al, Cu, Sn, and C.[1,6–13] From these studies, solid solutions composed of $Ge_2Sb_2Te_5$ and C [i.e., $(Ge_2Sb_2Te_5)_{1-x}C_x$] have shown particular promise.[7–9,13–15] *Ab initio* calculations suggest that carbon, unlike most other elemental species, is capable of altering the tetrahedral bonding configurations of the amorphous $Ge_2Sb_2Te_5$. This change in configuration functionally necessitates greater energy to crystallize, thereby increasing the crystallization temperature.[5]

The increased crystallization temperatures of $(Ge_2Sb_2Te_5)_{1-x}C_x$ should seemingly come with a reduction in thermal conductivity.

All else being equal, a quaternary alloy has greater disorder than its three-component complement. Adding carbon should then increase the scattering of both charge and vibrational energy, thereby decreasing electrical and thermal conductivity. However, from a more fundamental perspective, carbon may have only a mild influence on thermal transport in crystalline phases owing to the high-level of anharmonicity exhibited by the cubic forms of $Ge_2Sb_2Te_5$.[16] With a high-level of anharmonicity, phonons will scatter with one another more readily than other sources such as alloying. Carbon alloying could, therefore, have a comparatively small impact on the thermal transport. Despite these competing perspectives, reports on $(Ge_2Sb_2Te_5)_{1-x}C_x$ have predominately focused on only electrical resistivity even though thermal transport is a key design parameter for $Ge_2Sb_2Te_5$ memory devices.[16]

In response, we examine the thermal conductivity and volumetric heat capacity of $(Ge_2Sb_2Te_5)_{1-x}C_x$ as a function of both carbon concentration and annealing temperature. Results are then interpreted by leveraging electrical resistivity measurements accompanied by structural characterization realized with Raman spectroscopy and x-ray diffraction (XRD). Beyond providing experimentally obtained thermophysical property values for $(Ge_2Sb_2Te_5)_{1-x}C_x$, the results underscore that the addition of carbon is effectively benign to thermal transport when the material has a comparable level of structural order to its three-component complement. More simply, carbon is of far more consequence to the phase stability than the thermal conductivity of $Ge_2Sb_2Te_5$ alloys in the amorphous phase as well as the cubic crystalline phase where anharmonicity of the lattice relegates alloy scattering to a secondary transport effect.

II. EXPERIMENTAL

Films of $(Ge_2Sb_2Te_5)_{1-x}C_x$ $(0 \leq x \leq 0.12)$ were synthesized via direct current magnetron sputter deposition within a Unifilm Co. PVD-300 system using targets supplied by Process Materials Inc. The chamber was evacuated to a base pressure of $<5 \times 10^{-7}$ Torr to establish a pristine deposition environment. The chamber was then back-filled with ultrahigh purity Ar (99.995%) used as the sputtering gas controlled at 10 mTorr during operation. Fused silica coupons, $1 \times 1\,cm^2$ in area, were utilized as the substrates. Select films were also deposited upon silicon (100) with a 400 nm thermal oxide, which were utilized for Raman spectroscopy and hot-stage XRD. Oxidized silicon and bulk fused silica provided favorable conditions for chalcogenide deposition and subsequent annealing. Deposition at low temperatures ($T < 60\,^{\circ}C$) onto amorphous substrates helped ensure an amorphous starting phase in the film and discouraged interdiffusion between film and substrate. With respect to the latter, cross-sectional transmission electron microscopy (TEM)/energy dispersive x-ray spectroscopy (EDS) showed no evidence for chemical reactions/inter-diffusion between film and substrate constituents even after films were annealed to temperatures $\geq 300\,^{\circ}C$. All TEM measurements took place using a FEI Titan G2 80–200 electron microscope operating at 200 kV that was equipped with a spherical aberration corrector on the probe-forming optics and four SuperXTM silicon-drift detectors.

Films exhibited a nominal thickness of 500 nm and varied in their fractional carbon concentrations of $x = 0$ to 0.12. Carbon concentrations were confirmed with wavelength-dispersive spectroscopy (WDS) using a JEOL JXA-8530F Field Emission Electron Probe Microanalyzer to a level within ± 0.5 at. % (x to within ± 0.005). For select concentrations, films were annealed in ambient atmosphere for 60 min with a hot plate at temperatures ranging from 50 to 350 °C. EDS was used to verify that the composition was spatially uniform before and after heating with no evidence of oxidation. Following the anneals, samples grown on fused silica were covered with a 120 nm layer of Au [adhered to the $(Ge_2Sb_2Te_5)_{1-x}C_x$ film with a 5 nm layer of Ti] to serve as an opto-thermal transducer for frequency-domain thermoreflectance (FDTR) measurements. Performing the Au/Ti deposition post-anneal avoids the potential for Ti diffusion and TiTe binary formation.[17] A corner of each sample was masked during chalcogenide deposition facilitating direct contact between the transducer and underlying silica substrate. This "witness" region allowed for direct measurement of the substrate thermal properties while providing a reference to deduce $(Ge_2Sb_2Te_5)_{1-x}C_x$ thickness from white light interferometry (see Fig. S1 of supplementary material).

Thermal conductivity was measured with FDTR, an optical pump–probe technique in which a modulated pump beam induces a periodic heating event at a sample surface. The resultant frequency-dependent temperature response is monitored with a concentrically focused probe laser through a proportional change in reflectivity. Most commonly in FDTR (and for this study), the phase difference between the pump and reflected probe signal is measured as a function of pump modulation frequency. The phase signal can then be analyzed with a multilayer heat diffusion model for which parameters of interest are determined through a nonlinear least squares regression. Further details of the technique and thermal model are detailed extensively in prior publications.[18–20]

Gold is used as the transducer as it is reflective at 532 nm and absorptive at 488 nm wavelengths, which correspond to the central wavelengths of the probe and pump beams, respectively. The emitted pump and probe powers were 6 and 8 mW, respectively. Knife-edge measurements of the focused spot sizes provided $1/e^2$ radii of $6.6 \pm 0.1\,\mu m$ (pump) and $5.8 \pm 0.1\,\mu m$ (probe). Measurements were recorded over a frequency range of 500 Hz−40 MHz.

The thermal model used to interpret the FDTR signal considered three layers consisting of an a-SiO_2 substrate, the $(Ge_2Sb_2Te_5)_{1-x}C_x$ film, and a capping layer of Au (with a 5 nm Ti adhesion layer). As the thickness of the Ti is very thin, it is considered as part of the Au/$(Ge_2Sb_2Te_5)_{1-x}C_x$ interface rather than a distinct layer. The $(Ge_2Sb_2Te_5)_{1-x}C_x$ thermal conductivity and volumetric heat capacity were treated as fitting parameters as was the thermal boundary conductance of the Au/$(Ge_2Sb_2Te_5)_{1-x}C_x$ interface. While the thermal boundary conductance between the Au/Ti and $(Ge_2Sb_2Te_5)_{1-x}C_x$ interface is left as an open parameter, we note that the thermal model has negligible sensitivity to the interface conductance, and it has little effect on the fitted values for the volumetric heat capacity and thermal conductivity (further details provided in the supplementary material). Furthermore, when thermal conductivity was in excess of $1\,W\,m^{-1}\,K^{-1}$, FDTR was insufficiently sensitive to the volumetric heat capacity and a constant value of $1.3\,MJ\,m^{-3}\,K^{-1}$ was used within the model.

Thermal measurements were supplemented with characterization of both the electronic transport and structure of the

$(Ge_2Sb_2Te_5)_{1-x}C_x$ films. Electrical conductivity was obtained using four-point probe measurements performed with a Jandel Engineering Limited Multiheight Probe on an additional set of films. To be clear, all measurements of electrical properties were completed at room temperature, including the heat-treated samples. The structural characteristics (i.e., phase, order, etc.) of the $(Ge_2Sb_2Te_5)_{1-x}C_x$ films, meanwhile, were examined as a function of carbon concentration and anneal temperature via a combination of Raman spectroscopy and XRD.

Raman measurements were performed leveraging a WiTec alpha300R system employing 532 nm light focused near its diffraction limit with a 50×/0.55 NA objective. Power was chosen to ensure that there was no laser induced changes in the material ($P < 120\,\mu$W). Collected light was dispersed onto a 2400 l/mm grating, resulting in a spectral accuracy of $<0.2\,\text{cm}^{-1}$. The Rayleigh filter precludes the collection of data at energies below $90\,\text{cm}^{-1}$. A representative spectrum from each film was acquired by averaging ~25 separate spectral acquisitions spaced over 1 mm. Spectral data were normalized to the measured intensity near $100\,\text{cm}^{-1}$ to facilitate comparative analysis.

Finer examination of the temperature-dependent phase transitions was realized via XRD measurements acquired *in situ* with heating. A Bruker D8 x-ray diffractometer configured with an incident-beam mirror optic coupled with a 500 μm pinhole collimator directed "light" toward an integrated XYZ stage to facilitate 2D XRD scans that were collected with a Vantec 2000 area-detector. Samples were heated in 5 °C steps from room temperature to 350 °C using a heating rate of ~10 °C/min that was controlled by a Materials Research Instruments (MRI) cryo-furnace equipped with a large beryllium dome window to maintain the $\sim 1 \times 10^{-4}$ Torr vacuum of the experiment. A step-and-hold data collection process was used to first heat the sample to a set temperature step where it was held while the XRD pattern was collected. XRD patterns were collected using fixed 2θ and ω-angles of 34 and 17°, respectively. This resulted in a 2θ range of 20°−55° for the XRD scans. The 2D nature of the data collection enabled analysis over a relatively large solid angle of the Debye ring that provided a $\pm 14°$ χ-integration when 2D frames were converted to 1D XRD patterns. Data collection times were typically 10–30 s per frame.

III. RESULTS AND DISCUSSION

The addition of carbon impacts the transport of both charge and heat. The acuteness of carbon's impact, in turn, is dependent on the temperature at which the film was annealed. At lower annealing temperatures (T < 140 °C), for example, the thermal conductivity is nearly identical among the films, regardless of the carbon content as shown in Fig. 1(a). Resistivity is increased slightly, with carbon addition in this regime being within an order of magnitude for all films [Fig. 1(c)]. Substantial differences emerge based on the carbon content, however, as the annealing temperature increases. Thermal conductivity ranges by as much as a factor of five. Resistivity, meanwhile, varies by up to six orders of magnitude. These trends are primarily a consequence of the variable phase stability that comes with the addition of carbon rather than the increased scattering it may impart. For example, not only does thermal conductivity of amorphous films remain relatively constant over the measured range of added carbon but so too do films annealed to the metastable face-centered cubic phase [see Fig. 1(b)]. To further support this claim, the following examines how phase stability impacts thermal transport in $(Ge_2Sb_2Te_5)_{1-x}C_x$ via the examination of the thermal results in tandem with structural characterization.

$Ge_2Sb_2Te_5$ transitions from an amorphous to a metastable face-centered cubic (fcc) crystalline structure at around 140 °C and then to a trigonal phase at temperatures exceeding 250 °C.[21–25] With order, comes more efficient transport. Thermal conductivity increases; resistivity decreases. This is apparent upon the examination of the carbon-free sample where "jumps" in thermal conductivity are observed at 140 and 250 °C accompanied by associated drops in resistivity. Quantitatively, the variations in thermal conductivity with annealing temperature for the carbon-free $Ge_2Sb_2Te_5$ are similar to previous reports by Lyeo *et al.*[21] The measured volumetric heat capacity, meanwhile, remains near a constant of $1.3\,\text{MJ m}^{-3}\,\text{K}^{-1}$ [Fig. 1(d)], which is similar to prior measurements from Lee *et al.*[22] The value also compares quite favorably to the $1.28\,\text{MJ m}^{-3}\,\text{K}^{-1}$ predicted by the Dulong–Petit limit, $\rho c_p \approx 3nk_B$, where k_B is the Boltzmann constant and n is the atomic number density assumed to be $3.09 \times 10^{22}\,\text{cm}^{-3}$, and the relation is applicable owing to the low Debye temperature (~100 K) of $Ge_2Sb_2Te_5$.[21,22]

Taken together, these correlations not only lend veracity to the thermal analysis but also provide insight into the carbon-dependent changes in thermal conductivity. For example, volumetric heat capacity remains constant with annealing temperature and is independent of the carbon content. Thermal conductivity, in contrast, is highly dependent on both when viewed across the full range of experimental test parameters [Fig. 1(a)]. A constant heat capacity implies that the chemical environment of the film does not change appreciably with the addition of carbon. More simply, $(Ge_2Sb_2Te_5)_{1-x}C_x$ behaves as an alloy as opposed to a composite. Consequently, variations in thermal conductivity with carbon can be attributed to variations in the scattering of the vibrational and charge carriers moving energy within the films. Scattering, in turn, will be affected by variations in order within the film as dictated by its phase, grain size, and other defects.

To assess order and phase, a combination of Raman spectroscopy and XRD was employed. At a high level, XRD probes the relative arrangement of atomic nuclei and, therefore, provides a deft means of deducing the phase. Raman is also capable of phase determination owing to symmetry of the normal modes of vibration, but in probing zone-center phonons is also sensitive to the scattering sources themselves (e.g., grains, impurities, etc).[26] The combination of methods, therefore, provides a means of assessing how the phase and scattering evolves with the annealing of $(Ge_2Sb_2Te_5)_{1-x}C_x$.

To examine phase evolution, principal component analysis (PCA) was used to analyze the temperature-dependent XRD data. Texture bias was minimized by integrating the 2D-XRD signal over a large χ-angle range and basing all PCA scores on several separate cubic diffraction peaks as highlighted in Figs. 2(a) and 2(b). Figure 2(c) provides the resulting fcc crystal volume fraction as a function of anneal temperature in which a value of one signifies nominally single phase fcc. However, due to some uncertainty

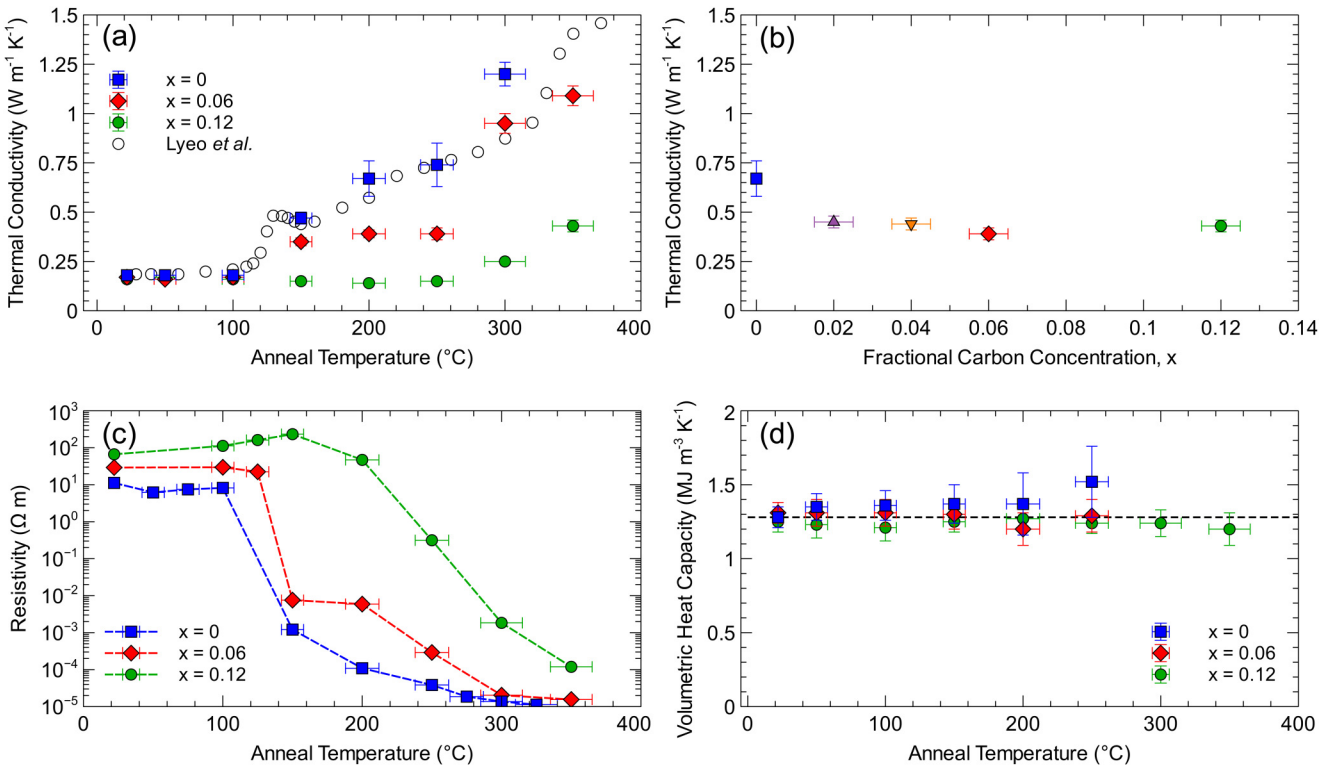

FIG. 1. (a) Thermal conductivity of $(Ge_2Sb_2Te_5)_{1-x}C_x$ films as a function of anneal temperature for $x = 0$, 0.06, and 0.12. For comparison, thermal conductivity measurements from Lyeo *et al.*[21] of $Ge_2Sb_2Te_5$ are displayed as white circles. The thermal conductivity as a function of carbon concentration is shown in (b) for films annealed into the fcc phase (films of $x \leq 0.06$ were annealed at 200 °C, and 350 °C for $x = 0.12$). (c) and (d) display the electrical resistivity and volumetric heat capacity as a function of anneal temperature. In (c), the dashed lines serve as a guide for the eye. The dashed line in (d) displays the expected volumetric heat capacity (1.28 MJ m^{-3} K^{-1}) in the Debye limit for *a*-$Ge_2Sb_2Te_5$, as calculated from the Dulong–Petit law. Thermal conductivity data in (a) are reprinted with permission from Lyeo *et al.*, Appl. Phys. Lett. **89**, 151904 (2006). Copyright 2006 AIP Publishing LLC.

within the factor score determination attributed to the aforementioned texture bias, values between 0.95 and 1 are effectively indistinguishable. For each of the films (having $x < 0.06$), an abrupt transition is observed in the range of 140 to 150 °C indicative of the transition from amorphous to crystalline. The onset of this phase transition moves to higher temperature with the addition of carbon owing to the greater phase stability that comes with the presence of carbon.[7–9,13–15] Enhanced crystalline phase stability is also seen in Fig. 2(c) as the range of temperature associated with single phase fcc broadens with added carbon.The reduction in fcc volume fraction that occurs at higher temperatures for films of lower carbon concentration is attributed to the emergence of the trigonal phase.

Comparison of the nominal phase fraction derived from XRD Fig. 2(c) and the transport data of Fig. 1 suggest that phase stability is not the sole cause for the carbon-dependent differences observed in thermal conductivity and electrical resistivity. For annealing temperature between 175 and 225 °C, for example, thermal conductivity and electrical resistivity vary appreciably even as films for which $x = 0-0.06$ are effectively completely transformed to their fcc form (and not yet trigonal). The influence of carbon must be affecting the scattering of the energy carriers in some way beyond just that induced by phase change.

This is apparent upon examination of the $(Ge_2Sb_2Te_5)_{1-x}C_x$ Raman spectra where appreciable differences are observed for films having similar XRD-derived phases but differing conductivities. Like that seen in the transport and XRD data, the Raman spectra [see Fig. 3(a)] are nearly identical across carbon concentrations at low annealing temperatures. Below 150 °C, the spectra are characteristic of an amorphous $Ge_2Sb_2Te_5$ owing to the broad feature at 155 cm^{-1} that stems from defective Sb–Te octahedra accompanied by a shoulder at 125 cm^{-1} originating from Ge–Te vibrations.[27] Higher annealing temperatures result in larger variations in the Raman spectra similar to the transport data. With annealing to 200 °C, Fig. 3(b), the highest carbon concentration ($x = 0.12$) persists in a Raman response characteristic of the amorphous phase. Lower carbon concentrations, in contrast, manifest broad features near 100 and 160 cm^{-1} associated with Sb–Te vibrations of the fcc phase accompanied by variable spectral weight in the 150 cm^{-1} region that could arise from residual amorphous regions. The carbon-free sample, meanwhile, exhibits an additional Raman mode at 175 cm^{-1} that only appears with annealing to higher

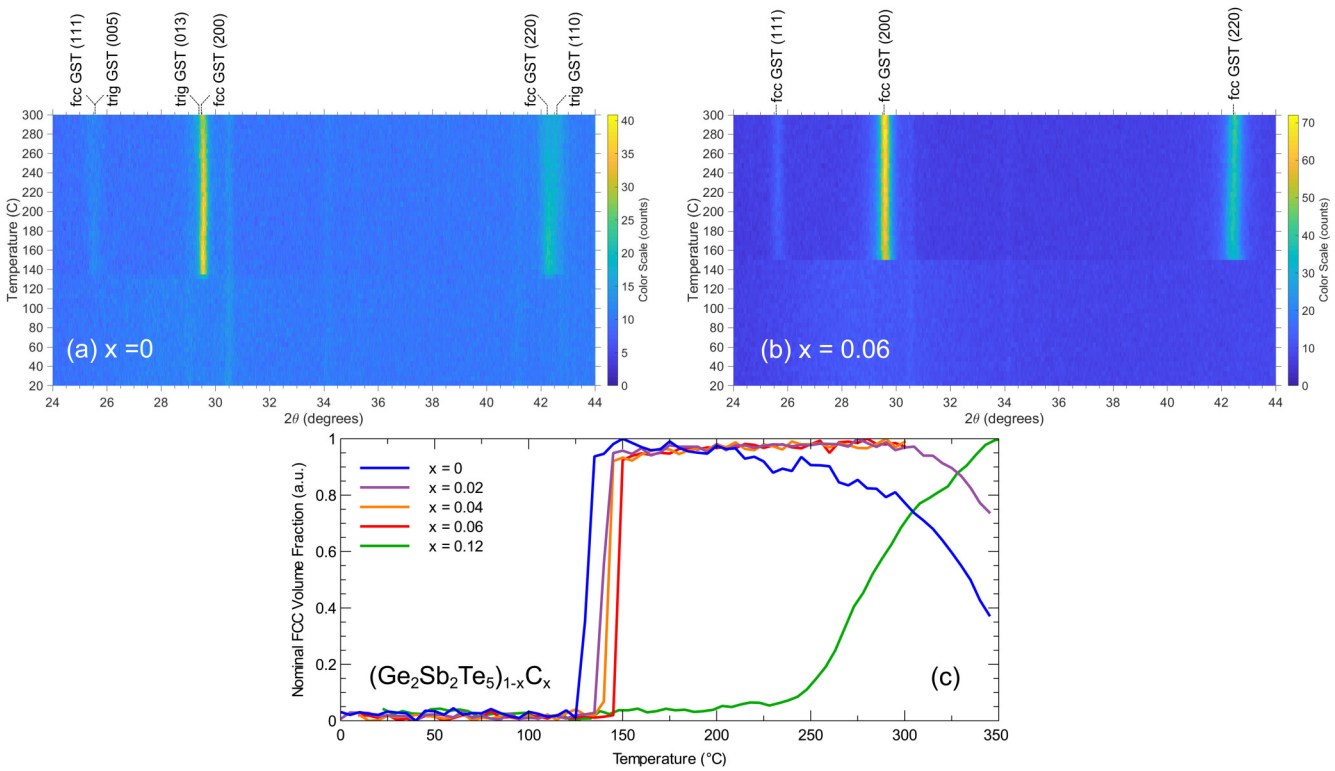

FIG. 2. (a) and (b) display representative x-ray diffractograms acquired during *in situ* heating of $(Ge_2Sb_2Te_5)_{1-x}C_x$ films. To minimize the impact of texturing on the deduction of the phase, several reflections were utilized in subsequent analysis. "GST" and "trig" are used as abbreviations for $(Ge_2Sb_2Te_5)_{1-x}C_x$ and trigonal, respectively. (c) Principal component analysis (PCA) was used to deduce the nominal fcc phase fraction as a function of temperature. Reductions at temperatures in excess of 200 °C indicate the onset of the trigonal phase transition.

temperatures for carbon containing films [see Fig. 3(c)]. This higher energy mode is attributed to trigonal Sb–Te bonds that are characteristic, but not necessarily indicative, of the second phase transition.

To quantify the observed differences in the Raman spectra, we define two ratios. First, the phase ratio was quantified by taking the quotient of the maximum intensity stemming from the strong fcc Sb–Te vibration near 100 cm^{-1} to the maximum response between 135 and 165 cm^{-1} corresponding to defective octahedra within the amorphous phase. Second, an order ratio is deduced by taking the proportion between the maximum Raman intensity between 165 and 195 cm^{-1}—a region containing both fcc and trigonal features—to the same "amorphous band" used in the phase ratio. We note that the order ratio is calculated for all concentrations except for $x = 0.12$, in which case, there is no peak formation corresponding to fcc and trigonal features. Functionally, each ratio is related to the relative strength of crystalline to amorphous spectral features. They are both empirical values whose magnitude is *not* indicative of any physical quantity but rather provides a means for comparison between films. They have each been named *ex post facto* owing to correlation with measurements of the phase and transport.

The phase ratio, for instance, shown in Fig. 3(d) exhibits a temperature dependence that closely correlates with the nominal phase fraction deduced from the XRD results of Fig. 2. The correlation is noteworthy on two fronts. First, it shows that the rudimentary nature of this "phase ratio" is capable of tracking the phase in $Ge_2Sb_2Te_5$ films. Second, it suggests that the order ratio is indicative of something beyond just the phase of the film.

Qualitatively, the order ratio assesses relative intensities of two closely spaced broad bands whose respective magnitudes will vary with linewidth. The linewidth is a direct measurement of a vibration's lifetime—and hence order—but is difficult to quantify with confidence for overlapping modes.[28] Thus, the intensity derived order ratio provides an indirect measurement of scattering apart from quantifying mode shape. Figure 3(e) plots the evolution of the order ratio with annealing temperature. Before the phase transition near 140 °C, the order ratio is practically equivalent between all films. However, with the phase change, the order ratio increases at different rates depending on carbon content. Specifically, the order ratio increases more rapidly for lower carbon content. However, unlike the phase transformation, variation in the order parameter is comparatively slow—compare the sudden "blips" in the XRD-derived fcc volume fraction and the Raman phase ratio with the meandering slope of the order ratio. This slower, carbon-dependent response, in turn, is similar to that seen in the transport data of Fig. 1. Taken together, the continued evolution of the order

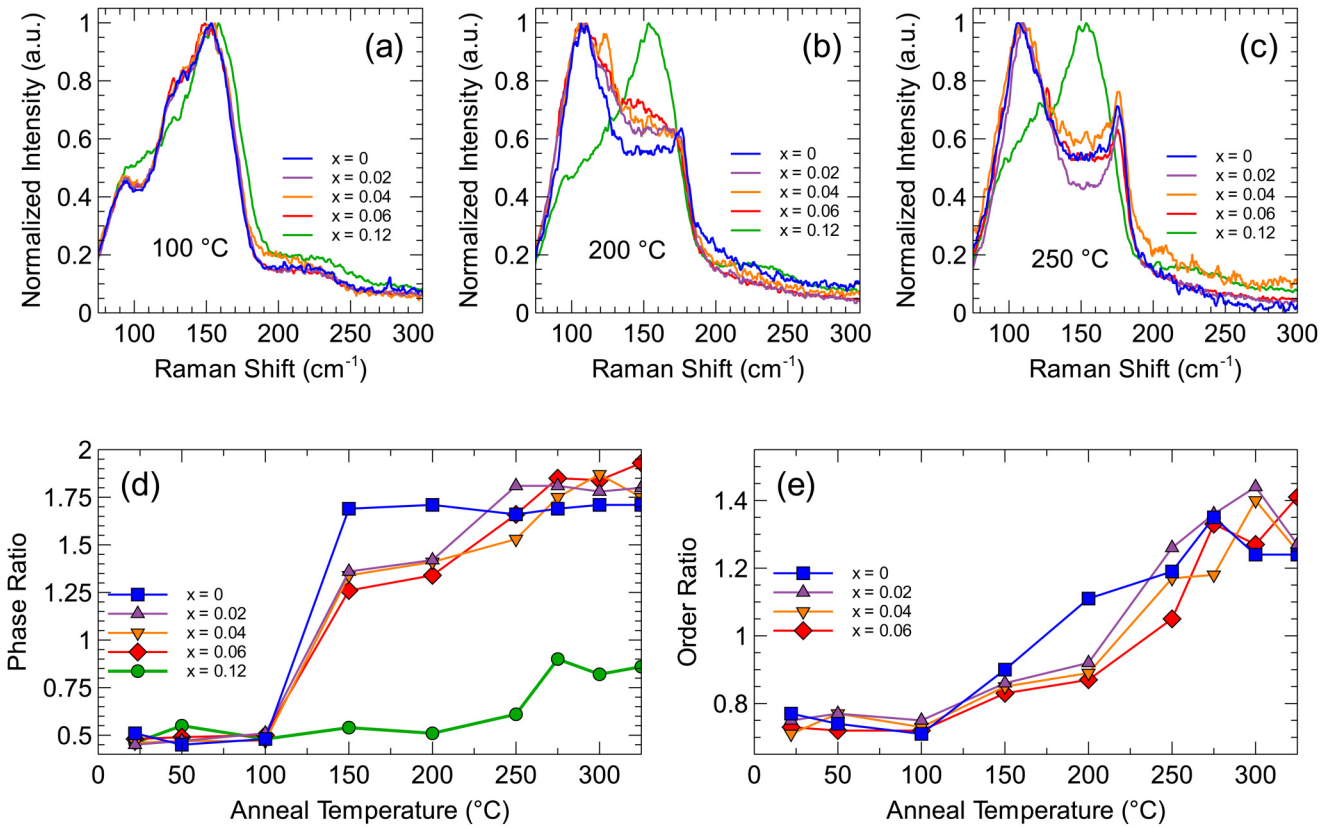

FIG. 3. Raman response of $(Ge_2Sb_2Te_5)_{1-x}C_x$ films annealed at (a) 100 °C (b) 200 °C, and (c) 250 °C. (d) Phase and (e) order ratio deduced from the Raman response as a function of anneal temperature.

ratio and the increasing thermal (electrical) conductivity with annealing even after the phase change suggests a continued "ripening" of the films that reduces scattering at a rate dependent on the carbon content.

Intuitively, carbon is an additional alloying element, and therefore, higher concentrations of added carbon will contribute to increased alloy scattering. Inspection of Figs. 1(a) and 1(b) suggests that more is at play, however. For example, at a given anneal temperature above 140 °C, there are observable differences in thermal conductivity between films of different carbon composition [Fig. 1(a)]; specifically, films with a lower concentration of added carbon have a higher thermal conductivity. However, little difference in thermal conductivity is observed between the films with added carbon once they are annealed to their fcc phase [Fig. 1(b)] as determined by PCA [Fig. 2(c)]. This suggests that the carbon content is not affecting the thermal (electrical) conductivity primarily through alloy scattering. Instead, carbon impacts the phase stability. The phase stability, in turn, dictates the order achieved with a given annealing temperature. More simply put, films having carbon are more disordered after annealing to a given temperature and thus have lower conductivity. By extension, if the same degree of order is achieved, conductivity will be nearly equivalent as alloy scattering from the carbon is playing a secondary role.

To support this conclusion, thermal conductivity is analyzed in its component parts—phonon and electron—under a similar paradigm to previous reports[21,29] and then compared to the order ratio. The electronic contribution to thermal conductivity can be calculated from the resistivity measurements through the Wiedemann–Franz law, in that

$$\kappa_e = LT\rho^{-1}, \tag{1}$$

where L is the Lorenz number, T is the temperature of the material, and ρ is the resistivity of the film. To account for potential variation in the Lorenz number, we bound our calculations by considering Lorenz numbers spanning from 1.5 to $2.44 \times 10^{-8}\,\mathrm{W\,\Omega\,K^{-2}}$, which provides a range representative of semiconductor materials.[30] The Sommerfeld value of the Lorenz number serves as an upper bound and is routinely applied for $Ge_2Sb_2Te_5$,[31–34] including films in the amorphous phase,[24,35] as well as for compositions of $Ge_2Sb_2Te_5$ with a quaternary addition.[35] A lower bound of $1.5 \times 10^{-8}\,\mathrm{W\,\Omega\,K^{-2}}$ is considered a converged limit for

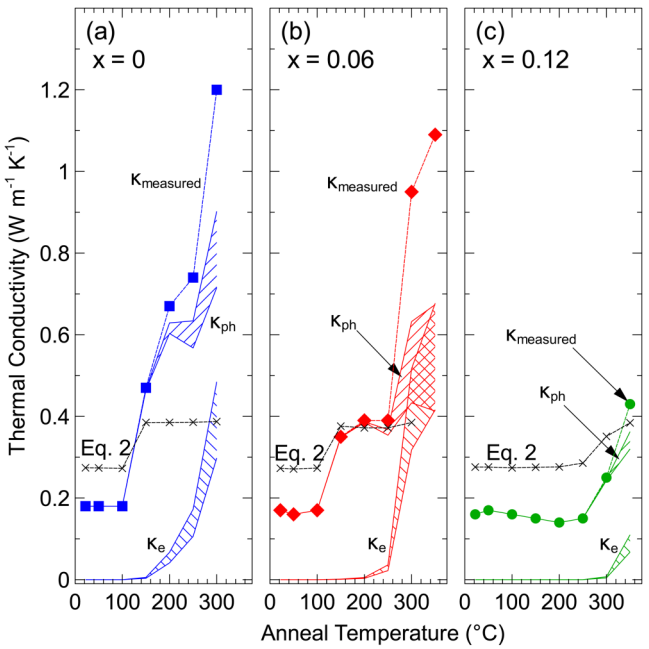

FIG. 4. Electron and phonon contributions to the film thermal conductivity as determined from FDTR and resistivity measurements. The range in values for κ_{ph} and κ_e account for variation in the Lorenz number. For comparison, the minimum limit to thermal conductivity is also displayed, as calculated according to Eq. (2).

non-degenerate semiconductors,[36] and has also been applied in several prior papers considering the electronic contribution to thermal conductivity in $Ge_2Sb_2Te_5$.[30,37] Following application of the Wiedemann–Franz law, the phonon contribution to thermal conductivity is then determined by taking the difference of the total measured thermal conductivity and that deduced from the electronic component, $\kappa_{measured} = \kappa_e + \kappa_{ph}$.

Figure 4 presents the deduced components of the thermal conductivity as a function of anneal temperature for $x = 0$, 0.06, and 0.12. When the film is in its amorphous state (low anneal temperature), transport is dictated by the vibrational component. In this regime, the thermal conductivity can be approximated by the Cahill–Swartz–Pohl minimum thermal conductivity limit in which the magnitude is defined by atomic density, and the speed of sound as given by

$$\kappa_{ph,min} = \frac{1}{2}\left(\frac{\pi}{6}\right)^{\frac{1}{3}} k_B n_a^{\frac{2}{3}} (v_l + 2v_t), \tag{2}$$

where k_B is the Boltzmann constant, n_a is the atomic density, and v_l and v_t are the longitudinal and transverse sound speeds within the film.[21,24] Details on the implementation of this calculation and the parameters used are provided in the supplementary material. With crystallization, this description of the vibrational component to thermal conductivity loses its validity. It does not account for the observed increase in thermal conductivity with anneal temperature that occurs at a rate dependent on carbon content. Rather, the increase indicates a reduction in scattering affecting both charge and vibration, implying increased order.

Ordering within $(Ge_2Sb_2Te_5)_{1-x}C_x$, in turn, is affected by the phase stability of the compound. Phase stability changes with the carbon content. More energy is required to get to the same level of order within the film when carbon is present. With the same level of order, however, transport effectively does not see the carbon. Figure 5 demonstrates this fact: the vibrational and electrical components to the thermal conductivity are each comparable irrespective of carbon content presuming that the same level of order has been achieved in the films. We again note that while the thermal conductivity is reduced for a given anneal temperature, this is

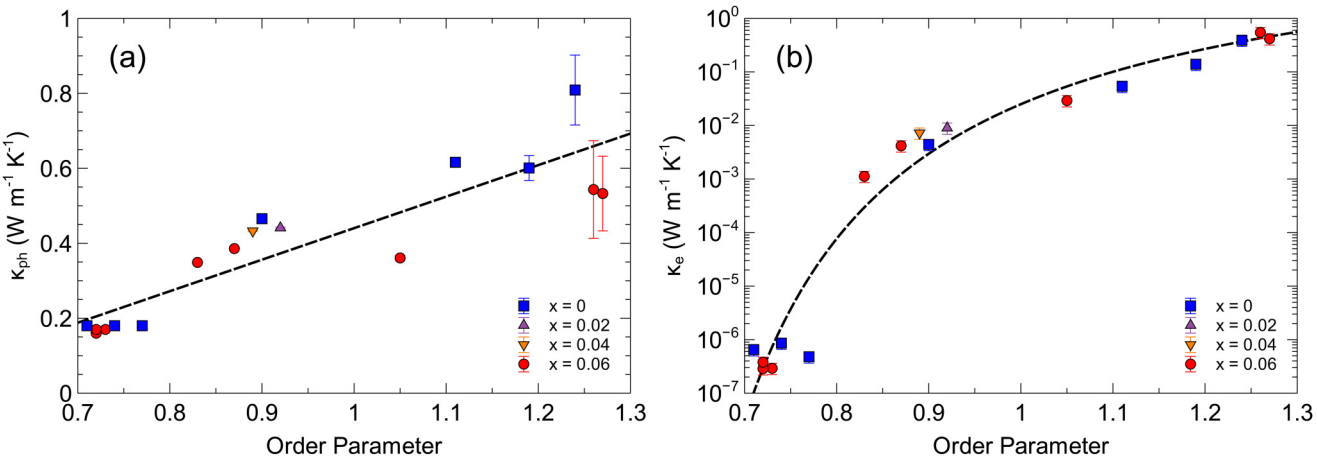

FIG. 5. (a) Phonon and (b) electrical contribution to thermal conductivity vs Raman derived order ratio. The error bars for κ_{ph} and κ_e account for variation in the Lorenz number. The dashed lines are provided as a guide to the eye.

attributable to a reduction in the order of the film. Once films of a higher carbon content are annealed to a level of similar order, comparable thermal conductivity is observed. Simply put, carbon does not impact the transport to an appreciable degree (for the specified range of x) as long as sufficient ordering of the films has occurred. In the language of transport, the presence of carbon is not the primary source of scattering. Rather, owing to the large anharmonicity of the $Ge_2Sb_2Te_5$ crystal lattice, phonon–phonon scattering likely occurs at such a high-rate that the alloy scattering caused by carbon is effectively inconsequential.[16]

IV. CONCLUSION

The thermal conductivity of $(Ge_2Sb_2Te_5)_{1-x}C_x$ films has been reported as a function of carbon concentration and anneal temperature using frequency-domain thermoreflectance. Trends in the thermal conductivity are closely correlated with modifications to structural evolution of the films as observed through Raman spectroscopy and XRD. Carbon does not act as a primary source of scattering to reduce thermal transport. Instead, it enhances the phase stability which necessitates increased annealing temperatures to achieve the same level of order. With similar levels of order, thermal conductivity of $(Ge_2Sb_2Te_5)_{1-x}C_x$ is comparable to the modest carbon concentrations examined here.

SUPPLEMENTARY MATERIAL

See the supplementary material for additional details on the white light interferometry measurements, measurement sensitivity analyses, and calculations of the electron and phonon contributions to thermal conductivity (and associated tabulated values).

ACKNOWLEDGMENTS

The authors thank the technical assistance and efforts of C. Sobczak, M. Abere, J. Griego, and P. Kotula. Thanks are also due to Amun Jarzembski of Sandia National Laboratories for critical review of this manuscript. P.E.H. appreciates support from the National Science Foundation (Grant No. 2006231). This work was performed under the Laboratory Directed Research and Development (LDRD) program at Sandia National Laboratories and undertaken, in part, at the Center for Integrated Nanotechnologies, an Office of Science User Facility operated for the U.S. Department of Energy (DOE) Office of Science. Sandia National Laboratories is a multimission laboratory managed and operated by National Technology & Engineering Solutions of Sandia, LLC, a wholly owned subsidiary of Honeywell International, Inc., for the U.S. DOE's National Nuclear Security Administration under Contract No. DE-NA-0003525. The views expressed in the article do not necessarily represent the views of the U.S. DOE or the United States Government.

DATA AVAILABILITY

The data that support the findings of this study are available from the corresponding author upon reasonable request.

REFERENCES

[1]E. M. Vinod, K. Ramesh, and K. S. Sangunni, "Structural transition and enhanced phase transition properties of Se doped $Ge_2Sb_2Te_5$ alloys," Sci. Rep. **5**, 1–7 (2015).
[2]K. Aryana, J. T. Gaskins, J. Nag, J. C. Read, D. H. Olson, M. K. Grobis, and P. E. Hopkins, "Thermal properties of carbon nitride toward use as an electrode in phase change memory devices," Appl. Phys. Lett. **116**, 043502 (2020).
[3]T. Nonaka, G. Ohbayashi, Y. Toriumi, Y. Mori, and H. Hashimoto, "Crystal structure of GeTe and $Ge_2Sb_2Te_5$ meta-stable phase," Thin Solid Films **370**, 258–261 (2000).
[4]P. Guo, A. M. Sarangan, and I. Agha, "A review of germanium-antimony-telluride phase change materials for non-volatile memories and optical modulators," Appl. Sci. **9**, 530 (2019).
[5]E. Cho, Y. Youn, and S. Han, "Enhanced amorphous stability of carbon-doped $Ge_2Sb_2Te_5$: Ab initio investigation," Appl. Phys. Lett. **99**, 183501 (2011).
[6]H. Horii, J. Yi, J. Park, Y. Ha, I. Baek, S. Park, Y. Hwang, S. Lee, Y. Kim, K. Lee *et al.*, "A novel cell technology using n-doped GeSbTe films for phase change RAM," in *2003 Symposium on VLSI Technology. Digest of Technical Papers (IEEE Cat. No. 03CH37407)* (IEEE, 2003), pp. 177–178.
[7]Q. Hubert, C. Jahan, A. Toffoli, G. Navarro, S. Chandrashekar, P. Noe, D. Blachier, V. Sousa, L. Perniola, J.-F. Nodin, A. Persico, R. Kies, S. Maitrejean, A. Roule, E. Henaff, M. Tessaire, P. Zuliani, R. Annunziata, G. Pananakakis, G. Reimbold, and B. De Salvo, "Lowering the reset current and power consumption of phase-change memories with carbon-doped $Ge_2Sb_2Te_5$," in *2012 4th IEEE International Memory Workshop* (IEEE, 2012), pp. 1–4.
[8]Q. Hubert, C. Jahan, A. Toffoli, G. Navarro, S. Chandrashekar, P. Noé, V. Sousa, L. Perniola, J.-F. Nodin, A. Persico, S. Maitrejean, A. Roule, E. Henaff, M. Tessaire, P. Zuliani, R. Annunziata, G. Reimbold, G. Pananakakis, and B. De Salvo, "Carbon-doped $Ge_2Sb_2Te_5$ phase-change memory devices featuring reduced RESET current and power consumption," in *2012 Proceedings of European Solid-state Circuits and Devices Conference (ESSDERC)* (IEEE, 2012), pp. 286–289.
[9]A. Kusiak, J.-L. Battaglia, P. Noé, V. Sousa, and F. Fillot, "Thermal conductivity of carbon doped GeTe thin films in amorphous and crystalline state measured by modulated photo thermal radiometry," J. Phys. Conf. Ser. **745**, 032104 (2020).
[10]S. Privitera, E. Rimini, and R. Zonca, "Amorphous-to-crystal transition of nitrogen- and oxygen-doped $Ge_2Sb_2Te_5$ films studied by in situ resistance measurements," Appl. Phys. Lett. **85**, 3044–3046 (2004).
[11]S. Raoux, M. Salinga, J. L. Jordan-Sweet, and A. Kellock, "Effect of Al and Cu doping on the crystallization properties of the phase change materials SbTe and GeSb," J. Appl. Phys. **101**, 044909 (2007).
[12]W. D. Song, L. P. Shi, X. S. Miao, and T. C. Chong, "Phase change behaviors of Sn-doped Ge–Sb–Te material," Appl. Phys. Lett. **90**, 091904 (2007).
[13]W. Zhou, L. Wu, X. Zhou, F. Rao, Z. Song, D. Yao, W. Yin, S. Song, B. Liu, B. Qian, and S. Feng, "High thermal stability and low density variation of carbon-doped $Ge_2Sb_2Te_5$ for phase-change memory application," Appl. Phys. Lett. **105**, 243113 (2014).
[14]X. Zhou, L. Wu, Z. Song, F. Rao, M. Zhu, C. Peng, D. Yao, S. Song, B. Liu, and S. Feng, "Carbon-doped $Ge_2Sb_2Te_5$ phase change material: A candidate for high-density phase change memory application," Appl. Phys. Lett. **101**, 142104 (2012).
[15]X. Zhou, M. Xia, F. Rao, L. Wu, X. Li, Z. Song, S. Feng, and H. Sun, "Understanding phase-change behaviors of carbon-doped $Ge_2Sb_2Te_5$ for phase-change memory application," ACS Appl. Mater. Interfaces **6**, 14207–14214 (2014).
[16]T. Matsunaga, N. Yamada, R. Kojima, S. Shamoto, M. Sato, H. Tanida, T. Uruga, S. Kohara, M. Takata, P. Zalden, G. Bruns, I. Sergueev, H. C. Wille, R. P. Hermann, and M. Wuttig, "Phase-change materials: Vibrational softening upon crystallization and its impact on thermal properties," Adv. Funct. Mater. **21**, 2232–2239 (2011).
[17]J.-L. Battaglia, A. Kusiak, A. Saci, R. Fallica, A. Lamperti, and C. Wiemer, "Effect of a thin Ti interfacial layer on the thermal resistance of $Ge_2Sb_2Te_5$-TiN stack," Appl. Phys. Lett. **105**, 121903 (2014).

[18]A. J. Schmidt, R. Cheaito, and M. Chiesa, "A frequency-domain thermoreflectance method for the characterization of thermal properties," Rev. Sci. Instrum. **80**, 094901 (2009).
[19]A. J. Schmidt, R. Cheaito, and M. Chiesa, "Characterization of thin metal films via frequency-domain thermoreflectance," J. Appl. Phys. **107**, 024908 (2010).
[20]J. Yang, C. Maragliano, and A. J. Schmidt, "Thermal property microscopy with frequency domain thermoreflectance," Rev. Sci. Instrum. **84**, 104904 (2013).
[21]H.-K. Lyeo, D. G. Cahill, B.-S. Lee, J. R. Abelson, M.-H. Kwon, K.-B. Kim, S. G. Bishop, and B.-K. Cheong, "Thermal conductivity of phase-change material $Ge_2Sb_2Te_5$," Appl. Phys. Lett. **89**, 151904 (2006).
[22]J. Lee, Z. Li, J. P. Reifenberg, S. Lee, R. Sinclair, M. Asheghi, and K. E. Goodson, "Thermal conductivity anisotropy and grain structure in $Ge_2Sb_2Te_5$ films," J. Appl. Phys. **109**, 084902 (2011).
[23]J. Lee, T. Kodama, Y. Won, M. Asheghi, and K. E. Goodson, "Phase purity and the thermoelectric properties of $Ge_2Sb_2Te_5$ films down to 25 nm thickness," J. Appl. Phys. **112**, 014902 (2012).
[24]J. Lee, E. Bozorg-Grayeli, S. Kim, M. Asheghi, H.-S. Philip Wong, and K. E. Goodson, "Phonon and electron transport through $Ge_2Sb_2Te_5$ films and interfaces bounded by metals," Appl. Phys. Lett. **102**, 191911 (2013).
[25]K. S. Siegert, F. R. L. Lange, E. R. Sittner, H. Volker, C. Schlockermann, T. Siegrist, and M. Wuttig, "Impact of vacancy ordering on thermal transport in crystalline phase-change materials," Rep. Prog. Phys. **78**, 013001 (2014).
[26]T. Beechem and S. Graham, "Temperature and doping dependence of phonon lifetimes and decay pathways in GaN," J. Appl. Phys. **103**, 093507 (2008).
[27]G. C. Sosso, S. Caravati, R. Mazzarello, and M. Bernasconi, "Raman spectra of cubic and amorphous $Ge_2Sb_2Te_5$ from first principles," Phys. Rev. B **83**, 134201 (2011).
[28]C. B. Saltonstall, T. E. Beechem, J. Amatya, J. Floro, P. M. Norris, and P. E. Hopkins, "Uncertainty in linewidth quantification of overlapping Raman bands," Rev. Sci. Instrum. **90**, 013111 (2019).
[29]C. D. Landon, R. H. T. Wilke, M. T. Brumbach, G. L. Brennecka, M. Blea-Kirby, J. F. Ihlefeld, M. J. Marinella, and T. E. Beechem, "Thermal transport in tantalum oxide films for memristive applications," Appl. Phys. Lett. **107**, 023108 (2015).
[30]W.-X. Song, Y. Cheng, D. Cai, Q. Tang, Z. Song, L. Wang, J. Zhao, T. Xin, and Z.-P. Liu, "Improving the performance of phase-change memory by grain refinement," J. Appl. Phys. **128**, 075101 (2020).
[31]D. Campi, E. Baldi, G. Graceffa, G. C. Sosso, and M. Bernasconi, "Electron–phonon interaction and thermal boundary resistance at the interfaces of $Ge_2Sb_2Te_5$ with metals and dielectrics," J. Phys. Condens. Matter **27**, 175009 (2015).
[32]X. Cai and J. Wei, "Thermal properties of Te-based phase-change materials," Proc. SPIE **8782**, 142–147 (2013).
[33]A. Faraclas, G. Bakan, L. Adnane, F. Dirisaglik, N. E. Williams, A. Gokirmak, and H. Silva, "Modeling of thermoelectric effects in phase change memory cells," IEEE Trans. Electron Devices **61**, 372–378 (2014).
[34]A. Vora-ud, M. Rittiruam, M. Kumar, J. G. Han, and T. Seetawan, "Molecular simulation for thermoelectric properties of c-axis oriented hexagonal GeSbTe model clusters," Mater. Des. **89**, 957–963 (2016).
[35]W. P. Risk, C. T. Rettner, and S. Raoux, Thermal conductivities and phase transition temperatures of various phase-change materials measured by the 3ω method," Appl. Phys. Lett. **94**, 101906 (2009).
[36]H.-S. Kim, Z. M. Gibbs, Y. Tang, H. Wang, and G. J. Snyder, "Characterization of lorenz number with seebeck coefficient measurement," APL Mater. **3**, 041506 (2015).
[37]R. Lan, R. Endo, M. Kuwahara, Y. Kobayashi, and M. Susa, "Electrical and thermal conductivity and conduction mechanism of $Ge_2Sb_2Te_5$ alloy," J. Electron. Mater. **47**, 3184–3188 (2018).